

EGFR is required for Wnt9a–Fzd9b signalling specificity in haematopoietic stem cells

Stephanie Grainger¹, Nicole Nguyen¹, Jenna Richter^{1,2}, Jordan Setayesh¹, Brianna Lonquich¹, Chet Huan Oon¹, Jacob M. Wozniak^{2,3,4}, Rocio Barahona¹, Caramai N. Kamei⁵, Jack Houston^{1,2}, Marvic Carrillo-Terrazas^{3,4}, Iain A. Drummond^{5,6}, David Gonzalez^{3,4}, Karl Willert^{1*} and David Traver^{1,7*}

Wnt signalling drives many processes in development, homeostasis and disease; however, the role and mechanism of individual ligand–receptor (Wnt–Frizzled (Fzd)) interactions in specific biological processes remain poorly understood. Wnt9a is specifically required for the amplification of blood progenitor cells during development. Using genetic studies in zebrafish and human embryonic stem cells, paired with in vitro cell biology and biochemistry, we determined that Wnt9a signals specifically through Fzd9b to elicit β -catenin-dependent Wnt signalling that regulates haematopoietic stem and progenitor cell emergence. We demonstrate that the epidermal growth factor receptor (EGFR) is required as a cofactor for Wnt9a–Fzd9b signalling. EGFR-mediated phosphorylation of one tyrosine residue on the Fzd9b intracellular tail in response to Wnt9a promotes internalization of the Wnt9a–Fzd9b–LRP signalosome and subsequent signal transduction. These findings provide mechanistic insights for specific Wnt–Fzd signals, which will be crucial for specific therapeutic targeting and regenerative medicine.

Wnt genes encode highly conserved, lipid-modified glycoproteins involved in the regulation of many developmental processes; yet, their specific functions are poorly understood. Although the mammalian genome encodes 19 Wnts and 10 Frizzled (Fzd) receptors, there is little evidence for signalling specificity through cognate Wnt–Fzd pairings¹. There is an exquisitely specific requirement for Wnt9a in directing an early amplification of haematopoietic stem and progenitor cells (HSPCs), a surprising finding because Wnts have been thought to be functionally promiscuous^{2–5}. Using HSPC development as a platform for validation, we demonstrate that the epidermal growth factor receptor (EGFR; also known as ERBB1) is required as a cofactor to mediate the specificity of the Wnt9a–Fzd9b signalling interaction, a finding that may indicate a general paradigm for Wnt–Fzd signalling specificity.

Haematopoietic stem cells (HSCs) are the tissue-specific stem cells that provide blood and immune cells for the duration of an organism's life. During development, these cells arise directly in major arterial vessels, from a specialized population of cells termed haemogenic endothelium (HE), specified from progenitors in the lateral plate mesoderm^{6,7}. HE cells receive inductive cues from nearby tissues, such as the somite and neural crest cells, including fibroblast growth factors, Notch and Wnt, to establish their fate and future function as HSPCs^{6–12}. After their specification, HSPCs emerge directly from the endothelium comprising the ventral floor of the dorsal aorta (hereafter aorta) in a process termed the endothelial-to-haematopoietic transition^{13,14}. They then enter the circulation and migrate to secondary haematopoietic organs, such as the fetal liver in mammals or the caudal haematopoietic tissue in teleosts, before seeding the final sites of residence in the bone marrow of mammals or the kidney marrow of teleosts^{6,7}.

Wnts are important to HSPC development and homeostasis^{15–26}. We previously determined that an early Wnt9a cue is specific in driving a proliferative event in the aorta, after HSCs have emerged, but before they have seeded the secondary haematopoietic organs. We hypothesized that this specific function of Wnt9a may be mediated through specific interaction with one of the 14 zebrafish Fzd receptors³.

Here, we identify Fzd9b as the cognate signalling partner for Wnt9a in the process of HSPC development, upstream of β -catenin, a process conserved in human haematopoiesis in vitro. Intracellular Fzd9b domains mediate the specificity of this Wnt–Fzd pairing, implicating a transmembrane spanning cofactor in establishing specificity. Using APEX2-mediated proximity labelling²⁷, we identified the receptor tyrosine kinase EGFR as being required for this specific signalling interaction. Altogether, these results demonstrate a conserved Wnt–Fzd pairing that mediates a precise Wnt cue required for haematopoiesis, shifting the paradigm of how specific Wnt–Fzd interactions are established and opening the field for discovery of other cofactors that mediate specific signalling through cognate Wnt–Fzd pairs.

Results

HSPCs require Fzd9b–Wnt9a interaction. Specificity of Wnt signals probably involves Wnt–Fzd pairings; we sought to identify a cognate Fzd for the specific Wnt9a signal, which occurs when the somite signals to ingressing HE precursors before 20h post-fertilization (hpf)³. A *fzd* expression screen in 16.5 hpf Fli1a⁺ (endothelial) cells indicated that a majority of genes encoding Fzds were expressed (Supplementary Fig. 1a,b). As the Wnt9a signal involves β -catenin³, we employed an established β -catenin-dependent Wnt

¹Department of Cellular and Molecular Medicine, University of California, San Diego, La Jolla, CA, USA. ²Biomedical Sciences Graduate Program, University of California, San Diego, La Jolla, CA, USA. ³Skaggs School of Pharmacy and Pharmaceutical Science, University of California, San Diego, La Jolla, CA, USA.

⁴Department of Pharmacology, University of California, San Diego, La Jolla, CA, USA. ⁵Massachusetts General Hospital Nephrology Division, Charlestown, MA, USA. ⁶Harvard Medical School, Department of Genetics, Boston, MA, USA. ⁷Section of Cell and Developmental Biology, University of California, San Diego, La Jolla, CA, USA. *e-mail: kwillert@ucsd.edu; dtraver@ucsd.edu

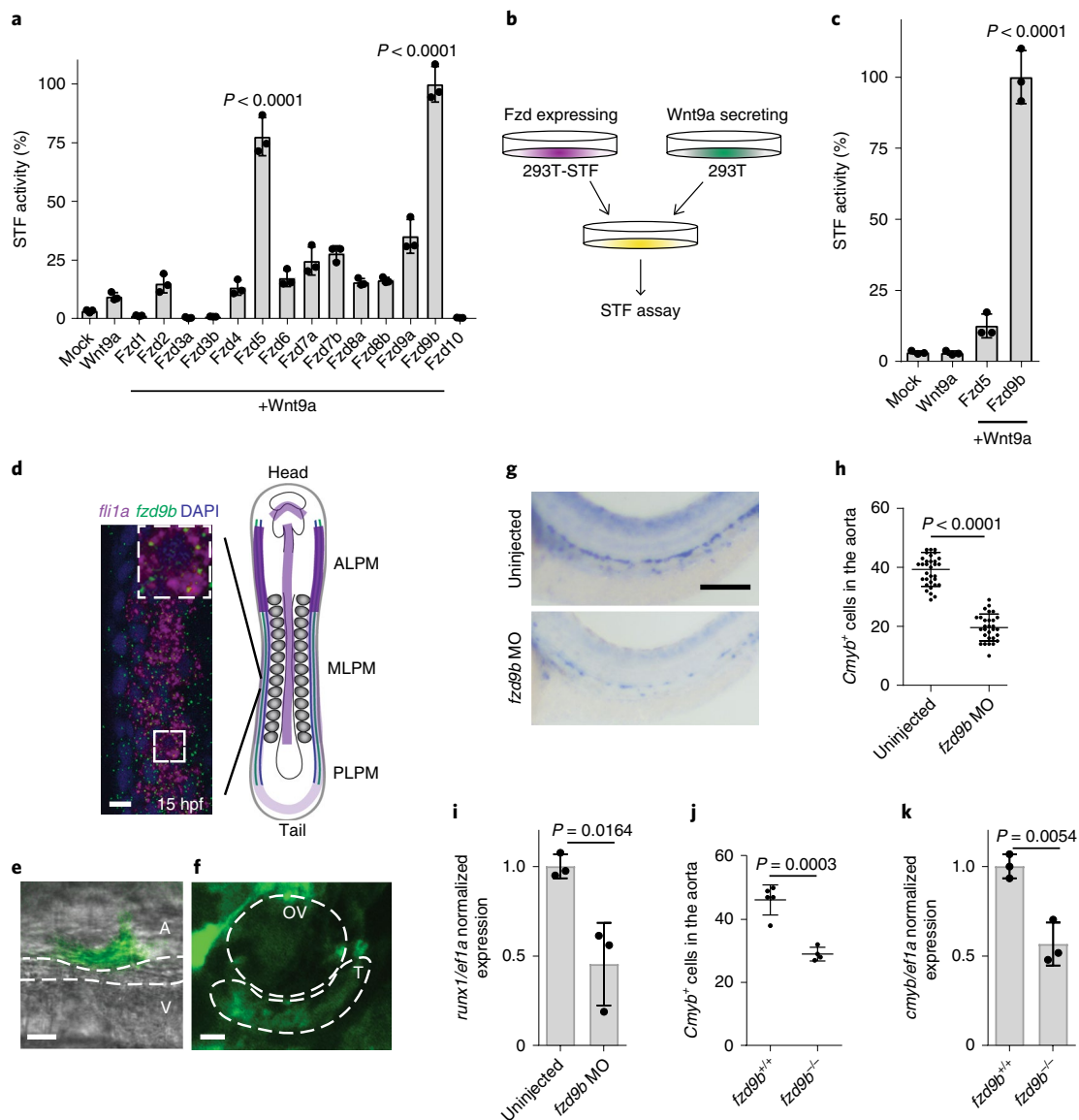


Fig. 1 | Fzd9b is required for zebrafish HSC development. **a**, STF assay screen with zebrafish Wnt9a (zWnt9a) and zFzds ($n=3$ biological replicates for each). **b,c**, zWnt9a cells were mixed with zFzd9b or zFzd5 STF cells and assayed for Wnt activity (**b**) and quantified in **c** ($n=3$ biological replicates for each). **d**, FISH for *fzd9b* (green) and *fli1a* (purple) in 15 hpf zebrafish embryos; DAPI is blue. ALPM, anterior lateral plate mesoderm; MLPM, medial lateral plate mesoderm; PLPM, posterior lateral plate mesoderm. Scale bar, 10 μ m. The diagram on the right shows haematopoietic precursors (green), vascular precursors (blue) and *fzd9b* expression (purple). **e**, Cells emerging from the aorta (A) labelled by *fzd9b:Gal4; UAS:GFP* at 40 hpf. V, vein. Scale bar, 10 μ m. **f**, Thymus (T) cells labelled by *fzd9b:Gal4; UAS:GFP* at 6 dpf. OV, otic vesicle. Scale bar, 25 μ m. **g,h**, WISH for *cmyb* at 40 hpf in *fzd9b* morphants and controls (**g**) and quantified in **h**. Each dot represents a biological replicate; $n=32$ control, $n=30$ MO (**h**). Scale bar, 30 μ m (**g**). In **d-g**, images are representative of 10 embryos examined in 3 independent experiments. **i**, qPCR for *cmyb* (black) and *runx1* in *fzd9b* morphants ($n=3$) and controls ($n=3$) at 40 hpf. **j**, Quantification of WISH for *cmyb* at 40 hpf in *fzd9b* mutants ($n=4$) and controls ($n=5$). Each dot represents a biological replicate. **k**, qPCR for *cmyb* in *fzd9b* mutants ($n=3$) and controls ($n=3$) at 40 hpf. In all graphs, the dots represent biological replicates from a single experiment, the bars represent the mean and the error bars represent the standard deviation. All STF assays were repeated independently with a similar trend. All qPCR data were generated from biological replicates from dissected trunks and tails. Statistical analyses were done by ANOVA compared to controls as indicated. NS, not significant.

reporter assay²⁸, called Super-TOP-Flash (STF), to identify Fzd candidates. STF reporter activity indicated a synergistic interaction between Wnt9a and Fzd5, or Wnt9a and Fzd9b, but no other Fzd (Fig. 1a and Supplementary Fig. 1c,d). Wnt9a signals to its cognate receptor on neighbouring cells, which we assessed using a co-culture approach (Fig. 1b). In this assay, Fzd9b, but not Fzd5, was able to transduce the Wnt9a signal and activate STF reporter activity (Fig. 1c), indicating that Fzd9b acts as a specific Wnt9a receptor. These observations were further supported by an absence of signal

using the Super FOP:FLASH reporter (a reporter lacking β -catenin activity; Supplementary Fig. 1e), and an absence of Fzd9b-specific signal in response to the prototypical ligand Wnt3a (Supplementary Fig. 1f). Altogether, these data provide evidence for a Wnt9a–Fzd9b interaction and indicate that Fzd9b is specifically involved in Wnt9a-mediated HSPC development.

Consistent with a role in Wnt9a signal reception, using fluorescent in situ hybridization (FISH), we found that at 15 hpf, *fzd9b* mRNA is co-expressed with the endothelial marker *fli1a* in the lateral

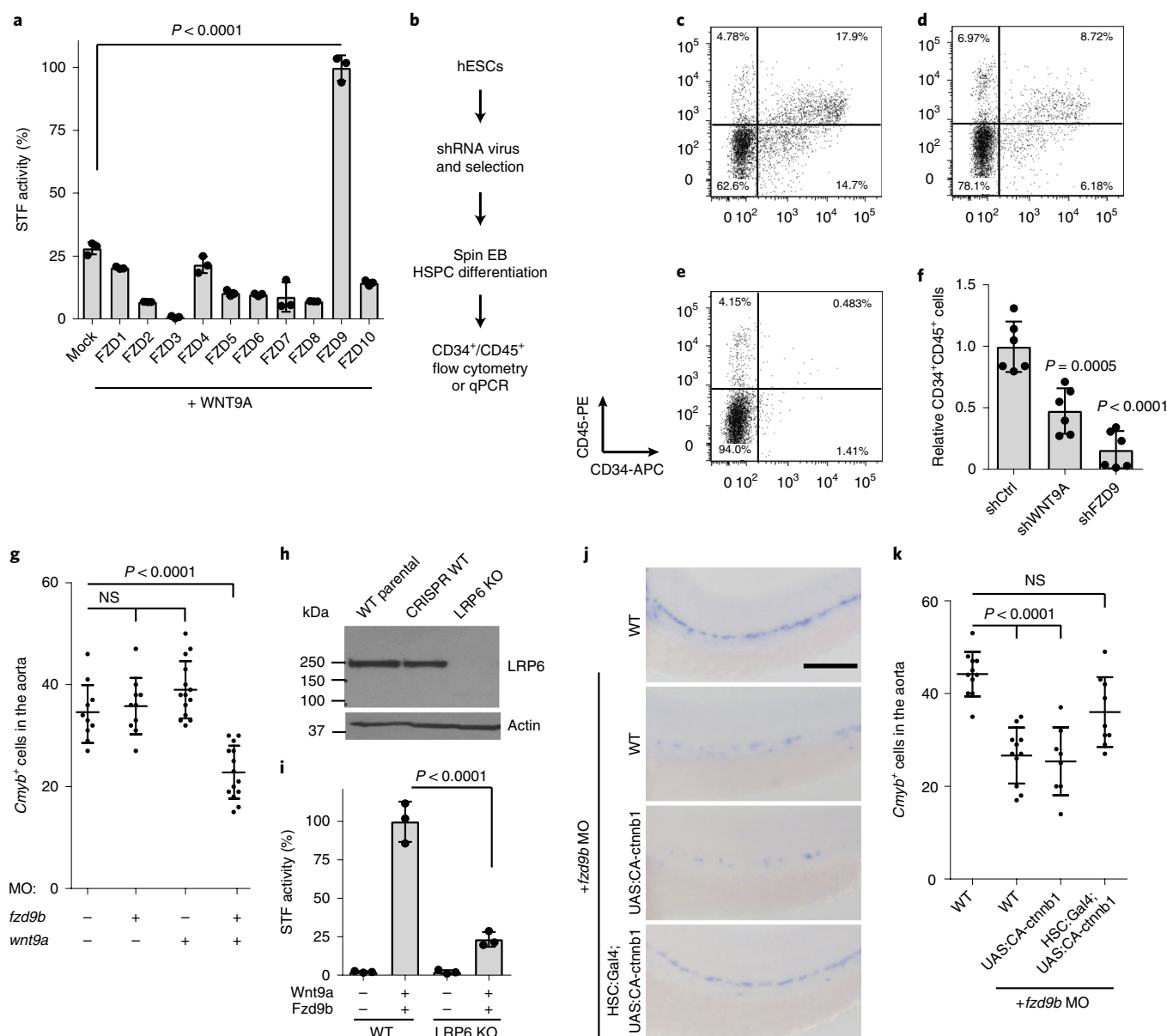


Fig. 2 | Fzd9b interacts genetically with Wnt9a. **a**, Quantification of the STF assay screen with human WNT9A and FZDs ($n = 3$ biological replicates each). **b**, Schematic of the experimental design for HSPC derivation. EB, embryoid bodies; hESCs, human embryonic stem cells. **c–f**, Representative flow cytometry plots of CD34 versus CD45 cells after 14 d of differentiation towards HSPCs in shControl (**c**), shWNT9A (**d**) and shFZD9 (**e**) transduced cells. Note the loss of double-positive cells with the loss of WNT9A or FZD9, quantified in **f** ($n = 6$ biological replicates each). **g**, Quantification of WISH for *cmyb* in suboptimal MO (0.1 ng *wnt9a* and 0.5 ng *fzd9b*) treated zebrafish at 40 hpf; $n = 10, 10, 14$ and 14 biological replicates from left to right. **h**, LRP6 immunoblot of lysates from wild-type HEK293T STF cells (WT parental), CRISPR-treated cells without disruption of LRP6 (CRISPR WT) and a LRP6-null mutant line (LRP6 KO). The image is representative of four experimental replicates. **i**, STF activity in WT and LRP6 KO HEK293T STF cells transfected with zWnt9a and zFzd9b. $n = 3$ biological replicates for each. **j**, WISH for *cmyb* at 40 hpf in WT, UAS:CA-ctnnb1 and *gata2b:Gal4;UAS:CA-ctnnb1*, injected with *fzd9b* MO. Scale bar, 30 μm . **k**, Quantification of **j**; $n = 11, 11, 8$ and 9 biological replicates from left to right. In all graphs, each dot represents a biological replicate from a single experiment, bars represent the mean and the error bars represent the standard deviation. All STF assays were repeated independently with a similar trend. Statistical analyses were done by ANOVA compared to controls as indicated.

plate mesoderm, the tissue from which HE is derived^{6,7} (Fig. 1d). To test whether haematopoietic cells were derived from cells expressing *fzd9b*, we performed two lineage tracing experiments using *fzd9b* promoter sequences driving expression of Gal4. First, Gal4 activates an upstream activating sequence (UAS)-driven green fluorescent protein (GFP) (*fzd9b:Gal4; UAS:GFP*); second, UAS:Cre is activated to excise a loxP-flanked sequence encoding blue fluorescent protein (BFP), ultimately leading to expression of dsRed (*fzd9b:Gal4; UAS:Cre; loxP-BFP-loxP-dsRed*). Using this strategy, we were able to

observe GFP⁺ or dsRed⁺ (pseudo-coloured green in Supplementary Fig. 2a) cells in the floor of the dorsal aorta in the characteristic cup shape observed during the endothelial-to-haematopoietic transition (at 40 hpf), indicating that nascent HSPCs had expressed *fzd9b* prior to their emergence (Fig. 1e and Supplementary Fig. 2a, left). Thymocytes derived from HSCs reside in the thymus beginning around 4 d post-fertilization (dpf); these cells expressed GFP at 6 dpf and 7 dpf (Fig. 1f and Supplementary Fig. 2a, right), consistent with a function for *fzd9b* in HSPC development.

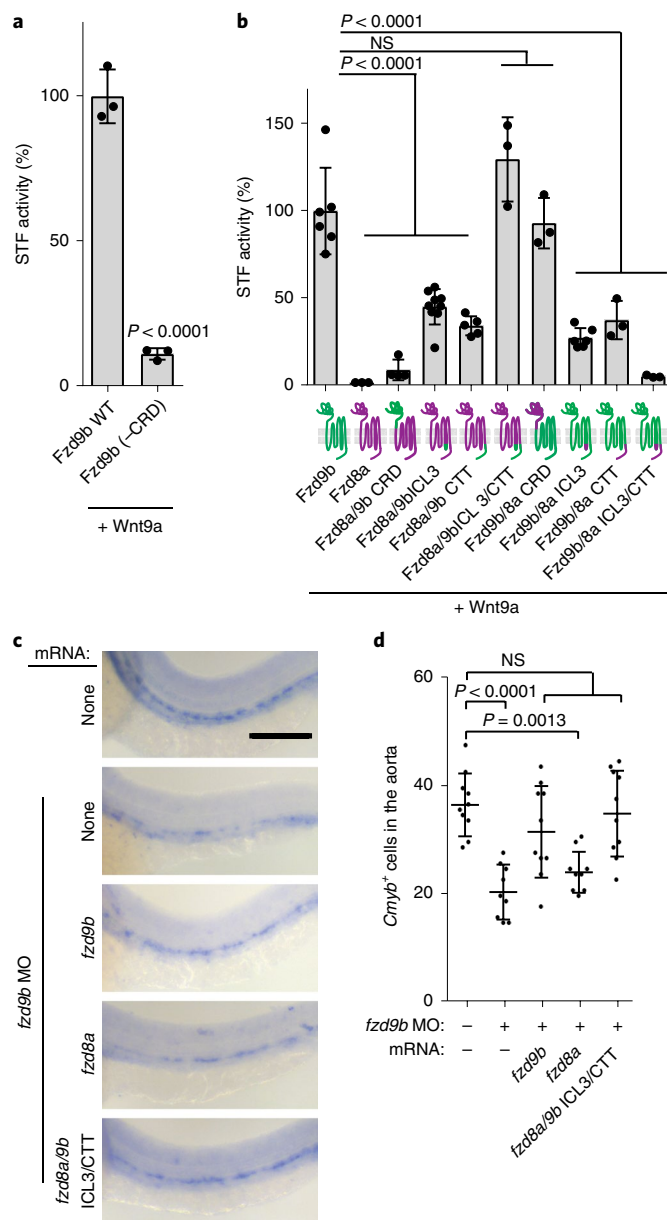


Fig. 3 | Wnt9a-Fzd9b specificity is mediated intracellularly. **a**, STF assay with zWnt9a and zFzd9b with and without the CRD ($n = 3$ biological replicates each). **b**, STF assay with zWnt9a and zFzd9b-zFzd8a chimaeras (schematics on the x axis: *zfd8a* is in magenta and *zfd9b* is in green); $n = 6, 3, 4, 9, 5, 3, 3, 6, 3$ and 3 biological replicates from left to right. **c**, WISH for *cmypb* at 40 hpf in *zfd9b* morphants injected with *zfd9b*, *zfd8a* and *zfd8a* mRNAs with ICL3 and CTT from *zfd9b* and uninjected control. Scale bar, 30 μm . **d**, Quantification of **c** ($n = 10, 9, 10, 9$ and 10 biological replicates from left to right). In all graphs, each dot represents a biological replicate, the bars represent the mean and the error bars represent the standard deviation. Panel **b** shows data from two experiments, whereas all other graphs represent biological replicates from the same experiment. All STF assays were repeated independently with a similar trend. Statistical analyses were done by ANOVA compared to controls as indicated.

To assess the function of Fzd9b in zebrafish HSPC development, we used an antisense morpholino (MO) oligonucleotide, which blocked translation of an ectopically provided Fzd9b-mKate fusion transcript in vivo (Supplementary Fig. 2b). Similar to *wnt9a* loss of function³, *zfd9b* morphants had normal specification, as mea-

sured by the early HSPC marker *runx1* (Supplementary Fig. 2c,d); however, HSPC expansion markers (*cmyb*, *gata2b* and *runx1*) were significantly reduced in *zfd9b* morphants at 40 hpf (Fig. 1g-i and Supplementary Fig. 2e,f). This loss of HSPCs persisted throughout development, where Rag1⁺ thymocytes were reduced in *zfd9b* morphants (Supplementary Fig. 2g). This effect was specific to HSPCs, as markers for the aorta (*dlc*, *dll4* and *notch1b*), vasculature (*kdr1*) and pronephros (*cdh17*) were normal (Supplementary Fig. 2h). The effects of the MO were specific, as the *zfd9b* MO could be rescued with *zfd9b* mRNA (Supplementary Fig. 2i,j), and two germline mutants of *zfd9b* (predicted to produce severely truncated proteins of approximately 30 residues) had reduced *Cmyb*⁺ cells at 40 hpf (Fig. 1j,k). Furthermore, MO-injected *zfd9b* mutants did not have a more severe phenotype than their siblings (Supplementary Fig. 2k). Finally, we used an established transgenic approach in which a guide RNA to *zfd9b* is expressed ubiquitously and *Cas9* (encoding CRISPR-associated protein 9) expression is spatially regulated to conditionally inactivate *zfd9b* in early endothelial cells²⁹, where the number of *Cmyb*⁺ cells at 40 hpf was also reduced (Supplementary Fig. 2l,m). Taken together with our finding that the Wnt signal is received by HE³, these results indicate that Fzd9b is required for HSPC development, downstream of fate specification, and specifically within HE.

Having identified a specific zebrafish Wnt9a-Fzd9b signal in vivo, we used the STF reporter assay and determined that only human FZD9 coupled effectively with WNT9A (Fig. 2a). Furthermore, using an established differentiation protocol to drive human embryonic stem cells towards haematopoietic fates³⁰ (Fig. 2b), we found that disrupting WNT9A or FZD9 expression using short hairpin RNAs (shRNAs) (Supplementary Fig. 3a,b) significantly compromised the ability of human embryonic stem cells to generate HSPCs, as assessed by flow cytometry for CD34 and CD45 (Fig. 2c-f) and by expression of endothelial (*CD34*) and haematopoietic markers (*CD31*, *CD45* and *CMYB*) (Supplementary Fig. 3c-f). These differences were not due to loss of pluripotency of the undifferentiated human embryonic stem cells, as they still abundantly expressed the pluripotency markers TRA1-81 and SSEA4 (ref. ³¹) (Supplementary Fig. 3g-i). Thus, Wnt9a-Fzd9b and WNT9A-FZD9 are required for both zebrafish and human HSPC development.

Fzd9b-Wnt9a operate upstream of β -catenin. To confirm that Wnt9a and Fzd9b function in the same pathway in vivo, we used genetic non-complementation with suboptimal MO dosages. A low dose of either *wnt9a* or *zfd9b* MO was not sufficient to affect HSPCs, whereas compound morphant animals had a reduction in the number of *Cmyb*⁺ cells similar to either *wnt9a* or *zfd9b* loss of function, supporting that these components operate in the same genetic pathway (Fig. 2g and Supplementary Fig. 4a).

The effect of Wnt9a on HSPCs required β -catenin (encoded by *ctnnb1*; or the canonical Wnt pathway)³, which relies on the assembly of Fzd-LRP5/6 heterodimers in response to a Wnt ligand¹. Consistent with this, the Wnt9a-Fzd9b signal could be synergistically increased in vitro in cells co-transfected with LRP6 (Supplementary Fig. 4b). To test the requirement for LRP6 in the Wnt9a-Fzd9b signal, we generated a HEK293T STF line deficient for LRP6 (Fig. 2h), which were compromised in their STF reporter activity following the addition of WNT3A (Supplementary Fig. 4c). Importantly, treatment with a glycogen synthase kinase 3 (GSK3) inhibitor (CHIR98014), which activates signalling independent of Wnt-Fzd-LRP interactions, stimulated STF activity, indicating that downstream signalling components were intact (Supplementary Fig. 4d). Wnt9a-Fzd9b signalling also required LRP6 (Fig. 2i), consistent with a role upstream of β -catenin. Accordingly, loss of *zfd9b*, the putative Wnt9a receptor, should be rescued by expression of constitutively active (CA) β -catenin. Indeed, HE-specific regulatory sequences (*gata2b* promoter) driving expression of CA- β -catenin

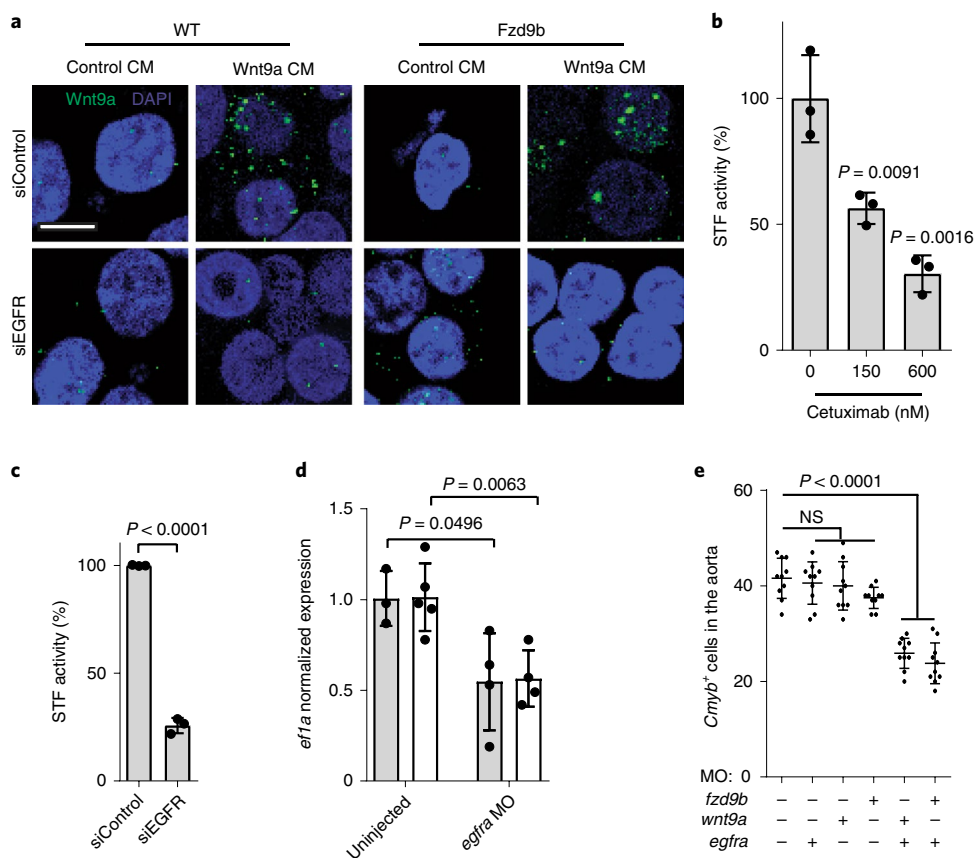


Fig. 4 | EGFR mediates Wnt9a-Fzd9b signalling. **a**, Immunofluorescence for zWnt9a in cells treated as shown. Scale bar, 15 μ m. Representative of ten fields of view from two experiments is shown. CM, conditioned medium. **b**, STF assay of zWnt9a and zFzd9b treated with cetuximab ($n=3$ biological replicates each). **c**, STF assay of zWnt9a and zFzd9b with siRNAs ($n=3$ biological replicates each). **d**, qPCR for *runx1* (grey) and *gata2b* (white) at 40 hpf generated from trunks and tails ($n=3, 5, 4$ and 4 biological replicates from left to right). **e**, Quantification of WISH for *cmyb* at 40 hpf (suboptimal MO dosages: 0.1 ng *wnt9a*, 0.5 ng *fzd9b* and 0.1 ng *egfra*); $n=11, 9, 10, 8, 10$ and 10 biological replicates from left to right. In all graphs, each dot represents a biological replicate from the same experiment, the bars represent the mean and the error bars represent the standard deviation. All STF assays were repeated independently with a similar trend. Statistical analyses were done by ANOVA compared to controls as indicated.

(CA-*ctnmb1*) was sufficient to rescue loss of *fzd9b* (Fig. 2j,k), indicating that Fzd9b functions upstream of β -catenin. Altogether, these data indicate that Wnt9a and Fzd9b function in the same genetic pathway, upstream of β -catenin.

Intracellular Fzd9b domains mediate specificity. How the Wnt-Fzd signalling complex relays its signal and establishes specificity is poorly understood, but is thought to rely on varying affinities of Wnts for the extracellular cysteine-rich domain (CRD) of Fzd^{1,32-34}. Using the STF assay system and zebrafish complementary DNAs, we found that, like other Wnts¹, the Fzd9b CRD is required to mediate the Wnt9a signal in vitro (Fig. 3a). Signalling differences were not due to differences in protein expression (Supplementary Fig. 5a).

We next sought to determine which domains are required for Wnt9a-Fzd9b signalling specificity by constructing a series of chimaeric Fzd transgenes between Fzd9b and Fzd8a, which is a Fzd that did not activate STF reporter activity with Wnt9a (Fig. 1a). Surprisingly, a chimaeric receptor in which the CRD of Fzd8a was replaced with that of Fzd9b did not signal (Fig. 3b), whereas the opposite chimaeric Fzd protein produced wild-type Wnt9a signalling activity (Fig. 3b), suggesting that other Fzd domains other than the CRD are critical determinants in Wnt9a-Fzd9b signalling specificity.

The signalling events downstream of the Wnt-Fzd-LRP interaction are thought to involve interaction with intracellular mediator proteins such as Dishevelled (Dsh; also known as Dvl), which

interacts with Fzd at the third intracellular loop (ICL3) and the carboxy-terminal tail (CTT)¹. Using further Fzd9b-Fzd8a chimaeras, we found that substituting both the ICL3 and the CTT from Fzd9b with those of Fzd8a was sufficient to completely ablate the signal, and the opposite was sufficient to produce wild-type signalling levels (Fig. 3b), whereas single substitutions resulted in partial levels of signalling (Fig. 3b), suggesting that signalling specificity for Wnt9a-Fzd9b lies entirely within the ICL3 and CTT domains. These chimaeras were expressed to the same level (Supplementary Fig. 5b), indicating that differences in signalling were not due to differences in expression. These findings were recapitulated using zebrafish and human cDNAs encoding chimaeras for Fzd9b-FZD9 and Fzd4-FZD4 (Supplementary Fig. 5c,d), indicating that the ICL3 and the CTT are required for zebrafish Fzd9b and human FZD9 signalling.

V5-tagged Fzd constructs had no change in the ability to mature or be modified post-translationally (Supplementary Fig. 5b), as assessed by their shift in size in immunoblots³⁵⁻³⁷. We also confirmed that the non-signalling chimaeric Fzd9bs were transported to the cell surface using immunofluorescence and flow cytometry with a Fzd9b antibody directed to the extracellular region between the CRD and the first transmembrane domain of Fzd9b (Supplementary Fig. 5d-f). Thus, differences in signalling were not due to differences in Fzd protein expression, maturation or transport to the cell surface.

Finally, to determine whether these domains were able to fulfil Fzd9b function in HSPC development, we co-injected *fzd9b*, *fzd8a*

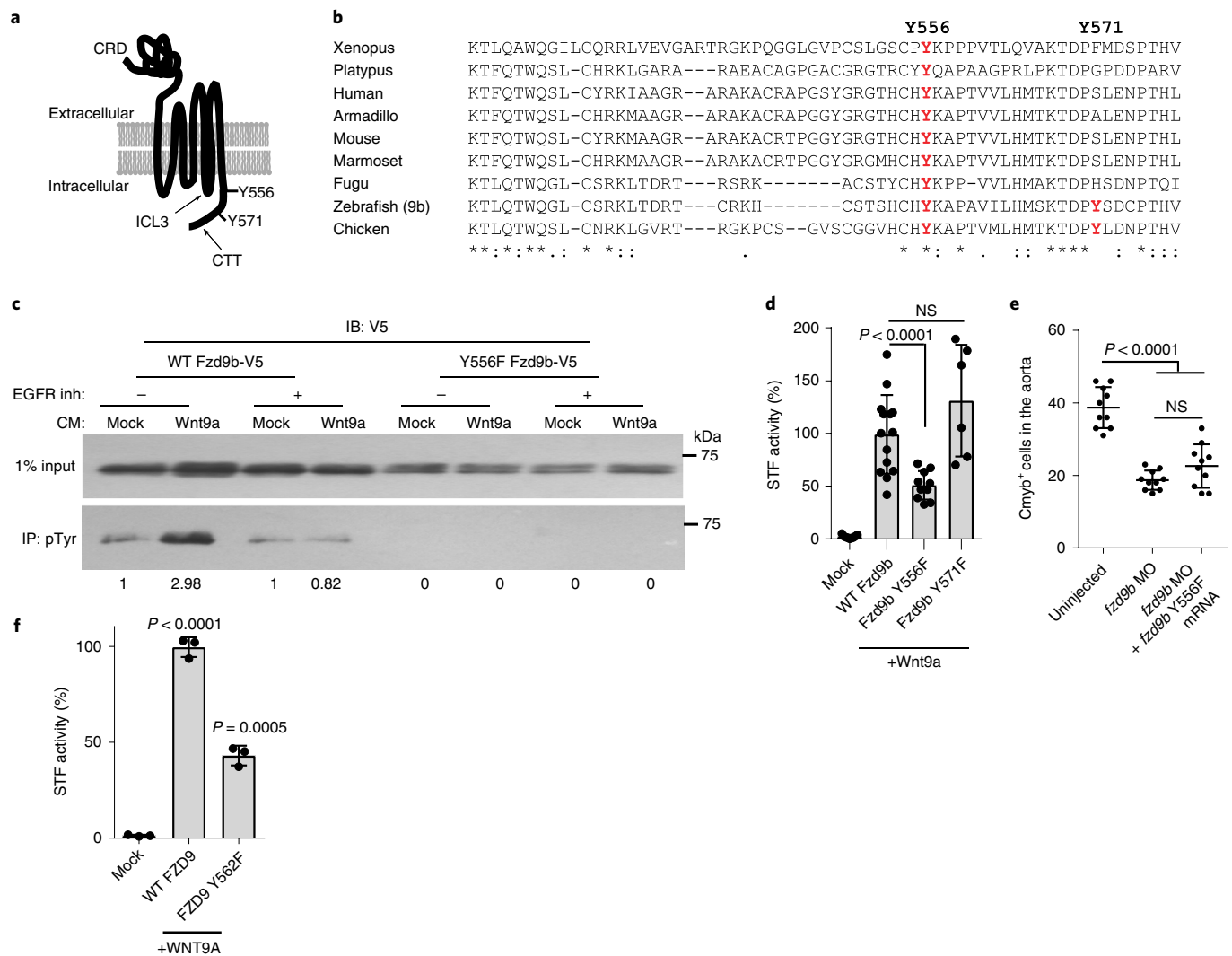


Fig. 5 | EGFR is required to phosphorylate the Fzd9b CTT in response to Wnt9a. **a**, zFzd9b protein with putative EGFR tyrosine phosphorylation sites. **b**, Protein alignment of Fzd9 CTTs from species shown, using ClustalOmega; * indicates complete conservation, : indicates conservation between highly similar residues, . indicates conservation with partially similar residues. **c**, Immunoblot (IB) for V5 from phosphotyrosine (pTyr) immunoprecipitation (IP) with increase in pY-zFzd9b (2.98 versus 1, arbitrary units). A trend was observed in four independent experiments. See also Supplementary Fig. 7. inh, inhibitor. **d**, STF assay of zFzd9b point mutants ($n = 9, 14, 10$ and 6 from left to right). **e**, Quantification of WISH for Cmyb⁺ cells in uninjected, *fzd9b* MO injected and *fzd9b* MO + *fzd9b* Y556F mRNA injected fish at 40 hpf ($n = 10$ zebrafish each). **f**, Quantification of the HEK293T cell STF assay with human WNT9A and FZD9 WT and Y562F mutant ($n = 3$ biological replicates each). In all graphs, the dots represent biological replicates from a single experiment, the bars represent the mean and the error bars represent the standard deviation. Statistical analyses were done by ANOVA compared to control as indicated. All STF assays were repeated independently with a similar trend.

or *fzd8a* mRNAs with the ICL3 and the CTT from *fzd9b* (*fzd8a/9b* ICL3/CTT) in the context of *fzd9b* MO, and found that only *fzd9b* and *fzd8a/9b* ICL3/CTT were able to rescue loss of *fzd9b* (Fig. 3c,d). Taken together, these data indicate that Wnt9a–Fzd9b specificity is regulated by the intracellular ICL3 and CTT domains of Fzd9b.

Wnt9a, Fzd9b and EGFR form a complex. As Wnt9a–Fzd9b specificity is mediated intracellularly, we postulated the existence of another signalling component that spanned the membrane to contact both Wnt9a and the intracellular portion of Fzd9b. Our ability to analyse Wnt9a–Fzd9b signalling specificity using zebrafish cDNAs in human cells further suggested that this signalling component would be highly conserved. To identify proteins that are in proximity to intracellular portions of Fzd9b, we generated a stable HEK293T cell line expressing Fzd9b fused via a glycine-serine linker to the peroxidase APEX2 (ref. ²⁷) (Fzd9b-5GS-APEX2). In the pres-

ence of hydrogen peroxide and biotin-phenol, endogenous proteins proximal to APEX2 (generally within 30 nm) are biotinylated within 1 min, allowing for their enrichment with streptavidin beads and subsequent identification by mass spectrometry (MS)²⁷. The Fzd9b-5GS-APEX2 cells, labelled specifically in the presence of biotin-phenol and hydrogen peroxide induction (Supplementary Fig. 6a), had correct Fzd9b localization (Supplementary Fig. 6b,c) and were able to signal in response to Wnt9a (Supplementary Fig. 6d).

Gene ontology (GO) analysis of the APEX-MS data revealed that in response to Wnt9a, the most changed biological processes included ERBB signalling (Supplementary Fig. 6e). Genes from the ERBB family encode single-pass transmembrane receptor tyrosine kinases that homodimerize and heterodimerize in response to multiple ligands to stimulate numerous signalling cascades³⁸. The transmembrane protein most enriched by proximity labelling was EGFR (Supplementary Fig. 6f). We hypothesized that EGFR may play a

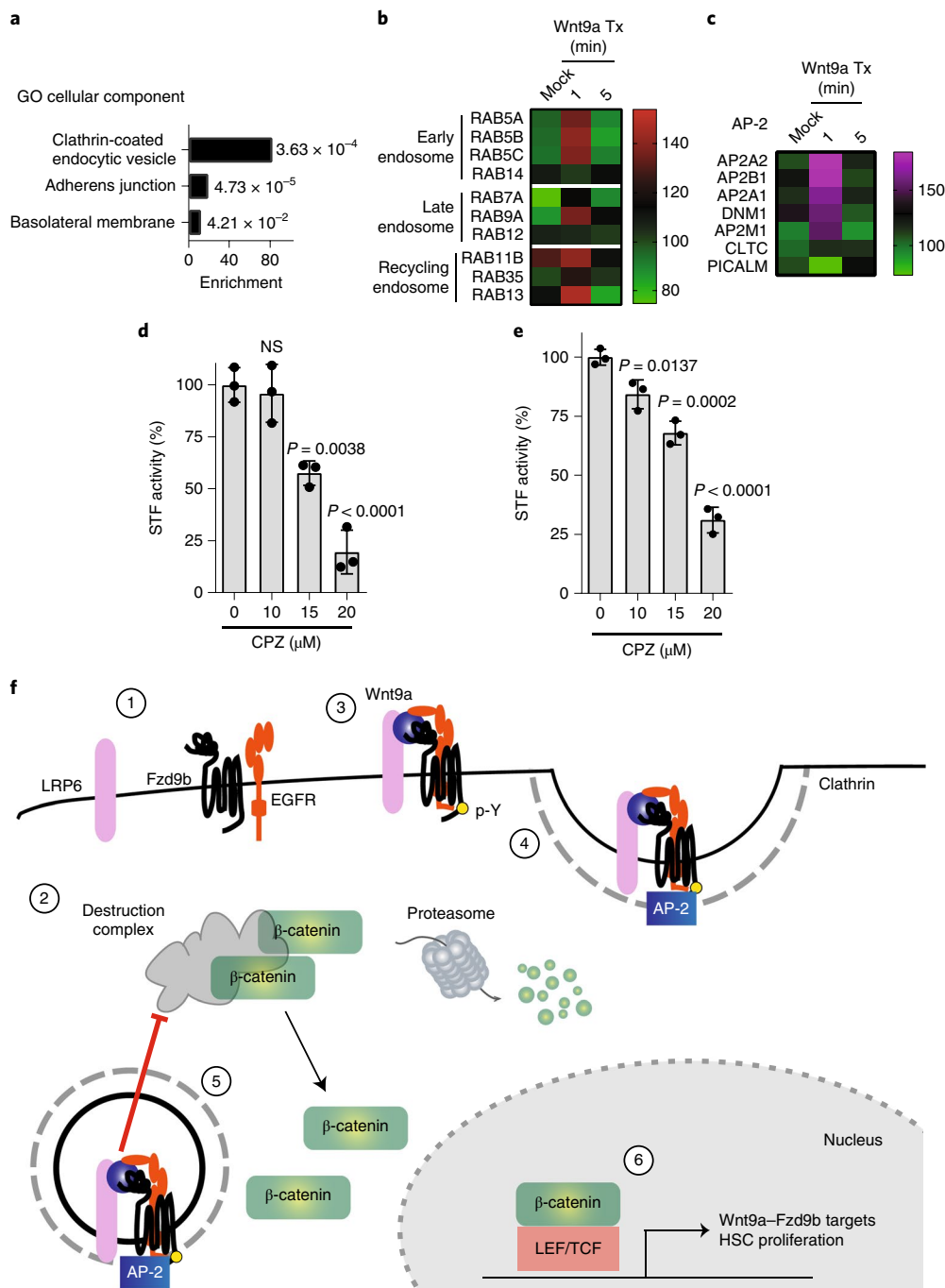


Fig. 6 | Clathrin-mediated endocytosis is required for the Wnt9a-Fzd9b signal. **a**, Fold enrichment of GO terms for cellular components identified from the top 5% of changed proteins in Fzd9b-APEX2 HEK293T cells treated with Wnt9a. The *P* values are listed next to each bar. *n* = 3 biological replicates. See Methods for analysis and statistics. **b**, Heatmap of Fzd9b-APEX2 proximity labelled normalized intensities of RAB members in the early endosome, late endosome and recycling endosome over time from *n* = 3 biological replicates. Tx, treatment. **c**, zFzd9b-APEX2 proximity labelled normalized intensity averages of three biological replicates. **d**, STF assay with zWnt9a and zFzd9b cultured with chlorpromazine (CPZ) (*n* = 3 experiments each). **e**, STF assay of hWNT9A CHO/hFZD9 STF co-culture treated with CPZ (*n* = 3 experiments each). In all graphs, the dots represent biological replicates from a single experiment, the bars represent the mean and the error bars represent the standard deviation. Statistical analyses were done by ANOVA compared to control as indicated. All STF assays were repeated independently with a similar trend. **f**, Fzd9b, LRP6 and EGFR are resident in proximity at the cell surface (1). The destruction complex targets β -catenin for degradation in the absence of a ligand (2). In the presence of Wnt9a, EGFR phosphorylates the Fzd9b tail at Y556 (3). AP-2 and clathrin are recruited (4). Fzd9b-LRP6 oligomerization leads to dissociation of the destruction complex and release of β -catenin into the cytosol, allowing for nuclear translocation (5). Nuclear β -catenin transactivates a programme for HSC proliferation (6).

role in Wnt9a recruitment to Fzd9b at the cell membrane. Indeed, disrupting EGFR expression in HEK293T cells stably expressing Fzd9b with short interfering RNA (siRNA) reduced cell-surface

binding of Wnt9a (Fig. 4a), suggesting that EGFR expression promotes Wnt9a binding to the cell surface. Interestingly, this also occurred in the absence of Fzd9b (Fig. 4a), suggesting that Wnt9a

binds directly to EGFR. In addition, treatment with cetuximab³⁹, which blocks the ligand binding to EGFR, dampened the Wnt9a–Fzd9b signal (Fig. 4b), consistent with a model in which EGFR forms a complex with Wnt9a and Fzd9b to transmit the Wnt signal.

HEK293T cells transfected with siRNA to EGFR compromised the ability of both zebrafish and human Wnt9a–WNT9A and Fzd9b–FZD9 to stimulate STF reporter activity (Supplementary Fig. 6g,h and Fig. 4c). Using a previously validated MO to *egfra*⁴⁰, the number of HSPCs at 40 hpf was decreased (Supplementary Fig. 6i,j), an effect that was validated with quantitative PCR (qPCR) (Fig. 4d), similar to the phenotypes of *fzd9b* or *wnt9a* loss of function, and consistent with a role for Egfr in regulating the Wnt9a–Fzd9b signal. Suboptimal MO dosing indicated that both Fzd9b and Wnt9a synergize genetically with Egfr during HSPC development (Fig. 4e). Furthermore, treatment of cells or zebrafish with the selective EGFR tyrosine kinase inhibitor AG1478 (ref. ⁴¹) significantly attenuated STF reporter activity or HSPC development, respectively (Supplementary Fig. 6k,m). Altogether, these data demonstrate that EGFR and its kinase activity are required for the Wnt9a–Fzd9b signal.

There are seven other known ligands for EGFR³⁸, which led us to hypothesize that these may be required to assemble EGFR, Wnt9a and Fzd9b into a complex. Of these, only heparin-bound EGF (HBEGF) is expressed in HEK293T cells⁴² (Supplementary Fig. 6n). To assess the requirement for HBEGF and other EGFR ligands in the Wnt9a–Fzd9b signal, we cultured HEK293T STF reporter cells in serum-free media lacking all known EGFR ligands and added a neutralizing antibody targeting HBEGF. STF reporter activity with Wnt9a–Fzd9b stimulation was maintained in these conditions (Supplementary Fig. 6o), indicating that this interaction occurs independently of known EGFR ligands.

The CTT of Fzd9b contains two tyrosine (Y) residues, at 556 and 571 (Fig. 5a), which are predicted to be potential kinase substrates⁴³. In addition, the Y556 on Fzd9b is highly conserved among vertebrates, indicative of putative functional importance (Fig. 5b). Consistent with these predictions, treatment with Wnt9a increased tyrosine phosphorylation of Fzd9b, which was dependent on EGFR kinase activity, as this increase was not observed in the presence of the EGFR tyrosine kinase inhibitor AG1478 (Fig. 5c). Furthermore, mutation of the Y556 (but not the Y571) sites decreased the in vitro signalling capacity of Wnt9a (Fig. 5d) and was not able to rescue *fzd9b* morphants (Fig. 5e); we also found that the corresponding residue in human FZD9, Y562F, is required (Fig. 5f). Together, these data indicate that Fzd9b is phosphorylated on Y556 in response to Wnt9a, which is required for its downstream signal.

EGFR is known to have effects on signal transduction, as well as receptor internalization and trafficking^{44–46}. Consistent with these functions, GO analysis of the APEX-MS data indicated that the most enriched cellular component was the ‘clathrin-coated endocytic vesicle’ (Fig. 6a). The APEX data also showed enrichment for proteins associated with early endosomes (RAB5A, RAB5B, RAB5C and RAB14), late endosomes (RAB7A, RAB9A and RAB12) and recycling endosomes (RAB11B, RAB35 and RAB13) (Fig. 6b), consistent with Fzd9b internalization in response to Wnt9a.

Internalization of transmembrane proteins can be mediated by clathrin-mediated or caveolin-mediated endocytosis, as can Fzd–Wnt complexes^{47,48}. The APEX-MS data indicated that the AP-2 complex and clathrin-mediated endocytosis machinery were recruited to Fzd9b in response to Wnt9a, suggesting that internalization was mediated by clathrin (Fig. 6c). Indeed, clathrin was required for both the zebrafish Wnt9a–Fzd9b and human WNT9A–FZD signals, as STF activity was reduced in the presence of the clathrin inhibitor chlorpromazine (Fig. 6d,e). These results indicate that Fzd9b is internalized and sorted through the endolysosome in response to Wnt9a.

Taken together, our data indicate a mechanism for the specificity of Wnt9a–Fzd9b signalling and a role for EGFR in directly regulating this Wnt signal. Fzd9b, LRP6 and EGFR are resident in proximity

at the cell surface (Fig. 6f, (1)); in the absence of a ligand, β -catenin is targeted for proteasomal degradation by the destruction complex (Fig. 6f, (2)); in the presence of Wnt9a, these are bridged, allowing EGFR-mediated phosphorylation of the Fzd9b tail at Y556 (Fig. 6f, (3)), leading to the recruitment of AP-2 and clathrin (Fig. 6f, (4)). Once inside the cell, Fzd9b–LRP6 oligomerization leads to dissociation of the destruction complex and the release of β -catenin (Fig. 6f, (5)). Finally, nuclear β -catenin transactivates a programme for HSC proliferation (Fig. 6f, (6)).

Discussion

One longstanding puzzle in the Wnt field has centred around the requirement for genetically encoding such a diverse set of ligands and receptors if Wnt ligands are as promiscuous as reported^{4,33,49}. The specificity dogma has been that Wnt–Fzd interactions are regulated by (1) physical binding affinities between Wnt and the Fzd CRD³², and (2) spatiotemporal localization, driven by the findings that different Wnt–Fzd combinations have different affinities and that many Wnts can physically interact with multiple (if not all) Fzd CRDs^{4,33,49,50}. In addition, (3) the ligand availability in the extracellular space is regulated by co-receptors, such as Reck and Gpr124 (refs. ^{51–54}), in a mechanism distinct from our findings. Our data indicate that signalling specificity is regulated at an additional level involving the activation of co-receptors. To this model, we propose the addition of (4) cofactors enzymatically activating Wnt–Fzd complexes for signalling through internalization. We hypothesize that different cofactors are recruited extracellularly by specific Wnt–Fzd pairs to target the receptor complex for signalling. These results support the notion that the specificity of Wnt–Fzd pairs relies on co-receptor complexes; however, the concept that Wnt stimulation recruits a co-receptor (EGFR), leading to its enzymatic regulation of the Fzd intracellular domains (tyrosine phosphorylation) and subsequent internalization for signalling, is unprecedented.

These discoveries have important implications in our understanding of development and disease, where overlapping functions of receptor tyrosine kinase families and Wnt, for example, may represent co-operative functions in signalling. Understanding Wnt–Fzd and cofactor-specific interactions will be critical to the advancement of regenerative medicine, such as in the development of protocols to derive different tissues in vitro from pluripotent precursor cells, where in large part, the requirement for β -catenin-dependent Wnt signalling in these protocols has been substituted with the prototypical ligand Wnt3a, or with GSK3 inhibitors, and not a specific ligand–receptor. Finally, determining how individual WNTs and FZDs are coupled will have important therapeutic implications, where pan-WNT inhibitory therapies cause toxic side effects. Furthermore, our observation that cetuximab, which blocks ligand binding to EGFR, disrupts Wnt9a–Fzd9b (WNT9A–FZD9 in humans) signalling suggests potential alternative mechanisms of action for this chemotherapeutic agent. Therapies targeting specific WNT–FZD pairs will allow for more precise targeting of these cancer cells.

Online content

Any methods, additional references, Nature Research reporting summaries, source data, statements of code and data availability and associated accession codes are available at <https://doi.org/10.1038/s41556-019-0330-5>.

Received: 27 September 2018; Accepted: 11 April 2019;
Published online: 20 May 2019

References

1. Nusse, R. & Clevers, H. Wnt/ β -catenin signaling, disease, and emerging therapeutic modalities. *Cell* **169**, 985–999 (2017).
2. Richter, J. et al. WNT9A is a conserved regulator of hematopoietic stem and progenitor cell development. *Genes (Basel)* **9**, E66 (2018).

3. Grainger, S. et al. Wnt9a is required for the aortic amplification of nascent hematopoietic stem cells. *Cell Rep.* **17**, 1595–1606 (2016).
4. Ring, L., Neth, P., Weber, C., Steffens, S. & Faussner, A. β -Catenin-dependent pathway activation by both promiscuous ‘canonical’ WNT3a–, and specific ‘noncanonical’ WNT4– and WNT5a–FZD receptor combinations with strong differences in LRP5 and LRP6 dependency. *Cell. Signal.* **26**, 260–267 (2014).
5. Voloshanenko, O., Gmach, P., Winter, J., Kranz, D. & Boutros, M. Mapping of Wnt–Frizzled interactions by multiplex CRISPR targeting of receptor gene families. *FASEB J.* **31**, 4832–4844 (2017).
6. Perlin, J. R., Robertson, A. L. & Zon, L. I. Efforts to enhance blood stem cell engraftment: recent insights from zebrafish hematopoiesis. *J. Exp. Med.* **214**, 2817–2827 (2017).
7. Clements, W. K. & Traver, D. Signalling pathways that control vertebrate haematopoietic stem cell specification. *Nat. Rev. Immunol.* **13**, 336–348 (2013).
8. Zhen, F., Lan, Y., Yan, B., Zhang, W. & Wen, Z. Hemogenic endothelium specification and hematopoietic stem cell maintenance employ distinct Scl isoforms. *Development* **140**, 3977–3985 (2013).
9. Leung, A. et al. Uncoupling VEGFA functions in arteriogenesis and hematopoietic stem cell specification. *Dev. Cell* **24**, 144–158 (2013).
10. Butko, E. et al. Gata2b is a restricted early regulator of hemogenic endothelium in the zebrafish embryo. *Development* **142**, 1050–1061 (2015).
11. Kobayashi, I. et al. Jam1a–Jam2a interactions regulate haematopoietic stem cell fate through Notch signalling. *Nature* **512**, 319–323 (2014).
12. Damm, E. W. & Clements, W. K. Pdgfr signalling guides neural crest contribution to the haematopoietic stem cell specification niche. *Nat. Cell Biol.* **19**, 457–467 (2017).
13. Kissa, K. & Herbomel, P. Blood stem cells emerge from aortic endothelium by a novel type of cell transition. *Nature* **464**, 112–115 (2010).
14. Bertrand, J. Y. et al. Haematopoietic stem cells derive directly from aortic endothelium during development. *Nature* **464**, 108–111 (2010).
15. Luis, T. C. et al. Wnt3a deficiency irreversibly impairs hematopoietic stem cell self-renewal and leads to defects in progenitor cell differentiation. *Blood* **113**, 546–554 (2009).
16. Zhao, C. et al. Loss of β -catenin impairs the renewal of normal and cml stem cells in vivo. *Cancer Cell* **12**, 528–541 (2007).
17. Fleming, H. E. et al. Wnt signaling in the niche enforces hematopoietic stem cell quiescence and is necessary to preserve self-renewal in vivo. *Cell Stem Cell* **2**, 274–283 (2008).
18. Reya, T. et al. A role for Wnt signaling in self-renewal of haematopoietic stem cells. *Nature* **423**, 409–414 (2003).
19. Willert, K. et al. Wnt proteins are lipid-modified and can act as stem cell growth factors. *Nature* **423**, 448–452 (2003).
20. Malhotra, S. et al. Contrasting responses of lymphoid progenitors to canonical and noncanonical Wnt signals. *J. Immunol.* **181**, 3955–3964 (2008).
21. Baba, Y. et al. Constitutively active β -catenin promotes expansion of multipotent hematopoietic progenitors in culture. *J. Immunol.* **177**, 2294–2303 (2006).
22. Kirstetter, P., Anderson, K., Porse, B. T., Jacobsen, S. E. & Nerlov, C. Activation of the canonical Wnt pathway leads to loss of hematopoietic stem cell repopulation and multilineage differentiation block. *Nat. Immunol.* **7**, 1048–1056 (2006).
23. Scheller, M. et al. Hematopoietic stem cell and multilineage defects generated by constitutive β -catenin activation. *Nat. Immunol.* **7**, 1037–1047 (2006).
24. Luis, T. C., Ichii, M., Brugman, M. H., Kincade, P. & Staal, F. J. Wnt signaling strength regulates normal hematopoiesis and its deregulation is involved in leukemia development. *Leukemia* **26**, 414–421 (2012).
25. Luis, T. C. et al. Canonical Wnt signaling regulates hematopoiesis in a dosage-dependent fashion. *Cell Stem Cell* **9**, 345–356 (2011).
26. Goessling, W. et al. Genetic interaction of PGE2 and Wnt signaling regulates developmental specification of stem cells and regeneration. *Cell* **136**, 1136–1147 (2009).
27. Lam, S. S. et al. Directed evolution of APEX2 for electron microscopy and proximity labeling. *Nat. Methods* **12**, 51–54 (2015).
28. Veeman, M. T., Slusarski, D. C., Kaykas, A., Louie, S. H. & Moon, R. T. Zebrafish prickle, a modulator of noncanonical Wnt/Fz signaling, regulates gastrulation movements. *Curr. Biol.* **13**, 680–685 (2003).
29. Ablain, J., Durand, E. M., Yang, S., Zhou, Y. & Zon, L. I. A CRISPR/Cas9 vector system for tissue-specific gene disruption in zebrafish. *Dev. Cell* **32**, 756–764 (2015).
30. Ng, E. S., Davis, R., Stanley, E. G. & Elefany, A. G. A protocol describing the use of a recombinant protein-based, animal product-free medium (APEL) for human embryonic stem cell differentiation as spin embryoid bodies. *Nat. Protoc.* **3**, 768–776 (2008).
31. Thomson, J. A. et al. Embryonic stem cell lines derived from human blastocysts. *Science* **282**, 1145–1147 (1998).
32. Janda, C. Y., Waghray, D., Levin, A. M., Thomas, C. & Garcia, K. C. Structural basis of Wnt recognition by Frizzled. *Science* **337**, 59–64 (2012).
33. Dijksterhuis, J. P. et al. Systematic mapping of WNT–FZD protein interactions reveals functional selectivity by distinct WNT–FZD pairs. *J. Biol. Chem.* **290**, 6789–6798 (2015).
34. Rulifson, E. J., Wu, C. H. & Nusse, R. Pathway specificity by the bifunctional receptor Frizzled is determined by affinity for Wingless. *Mol. Cell* **6**, 117–126 (2000).
35. Tamai, K. et al. LDL-receptor-related proteins in Wnt signal transduction. *Nature* **407**, 530–535 (2000).
36. Lawson, N. D. & Weinstein, B. M. In vivo imaging of embryonic vascular development using transgenic Zebrafish. *Dev. Biol.* **248**, 307–318 (2002).
37. Lewis, J. L. et al. Reiterated Wnt signaling during zebrafish neural crest development. *Development* **131**, 1299–1308 (2004).
38. Mishra, R., Hanker, A. B. & Garrett, J. T. Genomic alterations of ERBB receptors in cancer: clinical implications. *Oncotarget* **8**, 114371–114392 (2017).
39. Doody, J. F. et al. Inhibitory activity of cetuximab on epidermal growth factor receptor mutations in non small cell lung cancers. *Mol. Cancer Ther.* **6**, 2642–2651 (2007).
40. Zhao, Y. & Lin, S. Essential role of SH3-domain GRB2-like 3 for vascular lumen maintenance in zebrafish. *Arterioscler. Thromb. Vasc. Biol.* **33**, 1280–1286 (2013).
41. Osherov, N. & Levitzki, A. Epidermal-growth-factor-dependent activation of the src-family kinases. *Eur. J. Biochem.* **225**, 1047–1053 (1994).
42. Sultan, M. et al. Influence of RNA extraction methods and library selection schemes on RNA-seq data. *BMC Genomics* **15**, 675 (2014).
43. Blom, N., Gammeltoft, S. & Brunak, S. Sequence and structure-based prediction of eukaryotic protein phosphorylation sites. *J. Mol. Biol.* **294**, 1351–1362 (1999).
44. Schafer, B., Gschwind, A. & Ullrich, A. Multiple G-protein-coupled receptor signals converge on the epidermal growth factor receptor to promote migration and invasion. *Oncogene* **23**, 991–999 (2004).
45. Prenzel, N. et al. EGF receptor transactivation by G-protein-coupled receptors requires metalloproteinase cleavage of proHB-EGF. *Nature* **402**, 884–888 (1999).
46. Tomlins, S. A., Bollinger, N., Creim, J. & Rodland, K. D. Cross-talk between the calcium-sensing receptor and the epidermal growth factor receptor in Rat-1 fibroblasts. *Exp. Cell Res.* **308**, 439–445 (2005).
47. Yamamoto, H., Komekado, H. & Kikuchi, A. Caveolin is necessary for Wnt-3a-dependent internalization of LRP6 and accumulation of β -catenin. *Dev. Cell* **11**, 213–223 (2006).
48. Blitzer, J. T. & Nusse, R. A critical role for endocytosis in Wnt signaling. *BMC Cell Biol.* **7**, 28 (2006).
49. Yu, H., Ye, X., Guo, N. & Nathans, J. Frizzled 2 and Frizzled 7 function redundantly in convergent extension and closure of the ventricular septum and palate: evidence for a network of interacting genes. *Development* **139**, 4383–4394 (2012).
50. Hsieh, J. C., Rattner, A., Smallwood, P. M. & Nathans, J. Biochemical characterization of Wnt–Frizzled interactions using a soluble, biologically active vertebrate Wnt protein. *Proc. Natl Acad. Sci. USA* **96**, 3546–3551 (1999).
51. Cho, C., Smallwood, P. M. & Nathans, J. Reck and Gpr124 are essential receptor cofactors for Wnt7a/Wnt7b-specific signaling in mammalian CNS angiogenesis and blood–brain barrier regulation. *Neuron* **95**, 1221–1225 (2017).
52. Zhou, Y. & Nathans, J. Gpr124 controls CNS angiogenesis and blood–brain barrier integrity by promoting ligand-specific canonical Wnt signaling. *Dev. Cell* **31**, 248–256 (2014).
53. Eubelen, M. et al. A molecular mechanism for Wnt ligand-specific signaling. *Science* **361**, eaat1178 (2018).
54. Lai, M. B. et al. TSPAN12 is a norrin co-receptor that amplifies Frizzled4 ligand selectivity and signaling. *Cell Rep.* **19**, 2809–2822 (2017).

Acknowledgements

We thank C. Fine and J. Olvera for FACS assistance; R. Espin-Palazon, J. Nussbacher and I. J. Huggins for manuscript reading; I. J. Huggins for providing cetuximab; N. Gohad for microscopy assistance; and M. Boutros for cell lines. S.G. was supported by awards from the American Heart Association (14POST18340021) and the Leukemia and Lymphoma Society (5431-15). Research reported in this publication was supported by the National Heart, Lung, and Blood Institute of the US National Institutes of Health (NIH) under award number K99HL133458 (awarded to S.G.). The content is solely the responsibility of the authors and does not necessarily represent the official views of the NIH. J.R. was supported in part by the UCSD Interdisciplinary Stem Cell Training Program (CIRM TG2-01154) and by the American Heart Association Predoctoral Fellowship (16PRE27340012). This work was supported in part by funding to K.W. from the UCSD Stem Cell Program and was made possible in part by the CIRM Major Facilities grant (FA1-00607) to the Sanford Consortium for Regenerative Medicine. D.T. was supported by a Scholar Award (1657-13) from The Leukemia and Lymphoma Society and CIRM (RB4-06158). This project was also supported by the NIH/National Heart, Lung, and

Blood Institute grant R01HL135205 (awarded to D.T. and K.W.) and by the NIH/National Institute of General Medical Sciences grant R01GM110304 (awarded to K.W.). J.M.W. was supported by the Graduate Training in Cellular and Molecular Pharmacology Training Grant NIH T32 GM007752. I.A.D. was supported by the Harvard Stem Cell Institute and NIDDK grant UH2/3DK107372.

Author contributions

S.G. conceived, designed and conducted the experiments and analysis, and wrote the manuscript. N.N. and J.R. designed and conducted the experiments and analysis. J.S., B.L., R.B., C.H.O. and J.H. conducted the experiments and analysis. J.M.W., M.C.-T. and D.G. performed MS and conducted the analysis. C.N.K. and I.A.D. provided the zebrafish lines. D.T. and K.W. supervised the experiments and edited the manuscript.

Competing interests

The authors declare no competing interests.

Additional information

Supplementary information is available for this paper at <https://doi.org/10.1038/s41556-019-0330-5>.

Reprints and permissions information is available at www.nature.com/reprints.

Correspondence and requests for materials should be addressed to K.W. or D.T.

Publisher's note: Springer Nature remains neutral with regard to jurisdictional claims in published maps and institutional affiliations.

© The Author(s), under exclusive licence to Springer Nature Limited 2019

Methods

Cell culture and luciferase reporter assays. HEK293T cells or HEK293T cells lacking FZD1, FZD2 and FZD7 (kindly provided by M. Boutros, German Cancer Research Center) with a stably integrated STF⁵³ and Chinese hamster ovary (CHO) cells were grown in DMEM supplemented with 10% heat-inactivated FBS under standard conditions. HEK293T cells are known to have potential cross-contamination with HeLa cells (ICLAC Register of Misidentified Cell Lines (iclac.org/databases/cross-contaminations/)), which is irrelevant to this study.

For most assays, cells were seeded into six-well plates and transfected using polyethyleneimine (PEI), 50 ng *renilla* reporter vector, 200 ng cDNA expression vector, with a total of 1 µg DNA per well. For co-culture experiments, cells were passaged 24 h after transfection and plated together for analysis. For siRNA experiments, a well of a six-well plate was also treated with 10 pmol siRNA using RNAiMax transfection reagent (Invitrogen). All human WNT9A cell culture experiments except for the initial screen were performed by co-culturing stably expressing WNT9A CHO cells with stably expressing FZD9 HEK293T STF cells. Assays with Wnt3a were conducted in HEK293T cells lacking FZD1, FZD2 and FZD7 (ref. 5).

Serum-free conditions were established by gradually adapting our HEK293T STF reporter cells to SFM II (Invitrogen), which lacks all known EGFR ligands. Serum-free transfections were performed according to the manufacturer recommendations using Lipofectamine 3000. HBEGF neutralizing antibody (500 ng ml⁻¹; AF-259-SP, R&D systems) or normal goat serum (AB-108-C, R&D systems) were added 6 h after transfection.

All transfected cells were harvested 48-h post-transfection and all conditioned medium or co-cultured cells were harvested 24-h post-treatment; the lysates were processed and analysed using the Promega Dual Luciferase Assay System according to the manufacturer's instructions. Each experiment was performed with at minimum triplicate biological samples and reproduced at least once with a similar trend. Wnt activity was calculated by normalizing firefly luciferase output to Renilla luciferase; maximum fold induction was set to 100%. All STF reporter assays were conducted with a minimum of three biological replicates; the assays were always reproduced with a similar trend at least once.

Plates (10 cm) of HEK293T cells were transfected with 10 µg constructs encoding chimaeric Fzd cDNAs with a C-terminal V5 tag. For immunofluorescence, cells were plated onto glass coverslips after 24 h and stained with our Fzd9b antibody, generated to a region between the CRD and the first transmembrane domain, under non-permeabilized conditions, and according to standard protocols. For flow cytometry, cells were harvested with Accutase, pelleted, resuspended in PBS with 1% BSA and 1 mM EDTA, filtered through an 80-µm filter and sorted using a BD Fortessa flow cytometer. For immunoblots, cells were harvested 48 h after transfection in TNT buffer (1% Triton X-100, 150 mM NaCl and 50 mM Tris, pH 8) with protease inhibitors. Immunoblotting was performed according to standard procedures, using antibodies against V5 (1:5,000; GTX628529, GeneTex) and β-actin (1:20,000; A2228-100UL, Sigma).

For immunoprecipitation, cells were washed three times in PBS and lysed in RIPA buffer (10 mM Tris-HCl, pH 8, 10 mM EDTA, 0.5 mM EGTA, 1% Triton X-100, 0.1% deoxycholate, 0.1% SDS and 140 mM NaCl), supplemented with protease and phosphatase inhibitor tablets (Pierce) and 20 mM *N*-ethylmaleimide for 30 min at 4°C with rocking. Resultant lysates were cleared of cell debris by centrifugation at 15,000g for 10 min at 4°C and quantified by Bradford Assay. A minimum of 200 µg protein was diluted in 400 µl total volume with RIPA buffer; 2 µg antibody was added and incubated at room temperature for 30–60 min. Antibody–protein complexes were precipitated using Protein A Dynabeads (Invitrogen) for 30 min at room temperature, washed three times with 1 ml RIPA buffer and eluted using Laemmli buffer at room temperature. Precipitates were analysed by Fzd9b immunoblot. Immunoblot intensities from pull-downs were quantified by densitometry using ImageJ, normalized to input controls.

EGFR inhibition was performed using a 5 mM stock of AG1478 in 50:50 ethanol:dimethylsulfoxide. The final concentration used was 2.5 µM. Clathrin-mediated endocytosis was inhibited using chlorpromazine from a 1 M stock in 50:50 ethanol:dimethylsulfoxide. The final concentrations used are as indicated in the figure.

Wnt9a surface binding assay. Conditioned medium was collected from stably expressing Wnt9a or parental CHO cells and concentrated 10× using a 30-kDa molecular weight cut-off ultra-filtration device (Millipore). HEK293T cells stably expressing Fzd9b were transfected with control siRNA (siControl) or siEGFR and plated on 0.1% gelatin-coated glass coverslips after 24 h; after a further 24 h, cells were treated with cold conditioned medium for 3 h at 4°C, rinsed with PBS and fixed with 4% paraformaldehyde at 4°C for 20 min and at room temperature for 10 min. Immunofluorescence was performed using standard non-permeabilizing methods with a rabbit polyclonal antibody generated to zebrafish Wnt9a.

Generation of LRP6-knockout HEK293T STF line. A confluent 10-cm plate of HEK293T STF cells was transfected with 3 µg each of Cas9 and two guide RNAs under regulatory control of a U6 promoter. The guide RNAs (GGGCTTGAGGATGCAGCTG and GGATCTAAGGCAATAGCTCT) targeted the second exon of *LRP6*. Single-cell clones were validated for loss of LRP6

by sequencing the genomic locus, immunoblotting using a rabbit monoclonal antibody (1:1,000, C47E12; 2560S, Cell Signalling) and STF activity with mouse WNT3A, which requires LRP6 for signalling³⁵. Cell lines are available on request.

Fzd9b and Wnt9a antibody generation. Glutathione *S*-transferase fusion proteins for immunogens of Fzd9b (residues 115–226) and Wnt9a (residues 233–295) were purified by standard methods. Rabbits were immunized with glutathione *S*-transferase proteins, boosted and bled for serum according to standard methods (Lampire Biologicals). Antibodies against Wnt9a or Fzd9b were affinity purified against the same antigens fused to maltose-binding protein, according to the manufacturer's recommendations (Fisher), and stored in PBS/50% glycerol at –80°C. Antibodies are available on request.

Animals. Zebrafish were maintained and propagated according to the University of California and local Institutional Animal Care and Use Committee (IACUC) policies. AB⁺, *Tg(kdrl:Cherry-CAAX)¹⁷¹*, *Tg(fli1a:eGFP)¹⁵⁴⁴*, *Tg(cd5:Gal4)^{mu101}*, *Tg(UAS:CA-ctnmb1)^{sd47Tg}*, *Tg(gata2b:KalTA4)^{sd32}*, *UAS:Lifect:eGFP^{mu271}*, *wnt9a^{Δ28/Δ28,Δ49}*, *Tg(UAS:Cre)^{522Δ078}* and *Tg(bactin2:loxP-BFP-loxP-DsRed)^{sd27Tg}* lines have been previously described^{3,10,11,14,36,37}. For simplicity in the text, these lines are referred to with short forms listed in square brackets: *Tg(kdrl:Cherry-CAAX)* [*kdrl:mCherry*], *Tg(fli1a:eGFP)* [*fli1a:eGFP*], *Tg(UAS:CA-ctnmb1)^{sd47Tg}* [*UAS:CA-ctnmb1*], *Tg(gata2b:KalTA4)* [*HSC:Gal4*] and (*UAS:Lifect:eGFP*) [*UAS:eGFP*], *Tg(UAS:Cre)* [*UAS:Cre*], *Tg(bactin2:loxP-BFP-loxP-DsRed)* [*loxP BFP loxP dsRed*].

MO for *fzd9b* was targeted to block the ATG start codon with sequence 5'-AGGTGAGCTCCCATCTGATT-3' from GeneTools. One-cell-stage zygotes were injected with 2 ng *fzd9b* MO, and disruption of protein expression was confirmed with a fluorescently tagged mRNA. Suboptimal MO dosage was 0.5 ng. The *wnt9a* MO has been previously described³ and was used at 0.1 ng. The *egfra* MO has been previously described⁴⁰ and was used at 2.5 ng or 1 ng. Rescue experiments were performed using 20 pg *fzd* chimaeric mRNA synthesized using the SP6 mMessage machine kit (Ambion) according to the manufacturer's recommendations.

Clustered regularly interspaced short palindromic repeats (CRISPR)–Cas9 was used to generate germline mutants for *fzd9b*; single guide RNAs were chosen according to their ability to cleave DNA in vitro as previously described³⁶. Mutation of the *fzd9b* locus at the amino-terminal was achieved using 100 ng *cas9* mRNA (Trilink) and 100 ng single guide RNA (GGCTCTTATGACCTGGAGAG) and generated mutants with either a 2-bp insertion (*fzd9b^{2bp}*)^{b203} or a 7-bp deletion (*fzd9b^{7bp}*)^{b204}. For simplicity, in the text, these are referred to as *fzd9b^{-/-}*. Mutations were confirmed by sequencing individuals. Zebrafish lines are available on request.

Tg(fzd9b:Gal4) founders were established by injecting 25 pg of a Tol2 kit⁵⁷ generated plasmid with 100 pg transposase mRNA at the one-cell stage. The transgenic plasmid encoded a 4.3-kb *fzd9b* promoter region amplified using the primers: 5'-CTCCCATGAGGCAGACGTGTGT-3' and 5'-AGTCCGCGAGCAGCTTGCTGTT-3'; this was cloned into a p5E MCS Tol2 entry vector using XhoI and SacII restriction sites and then combined with a Gal4 middle entry and polyA 3' entry vector by Gateway assembly to make a full transgene construct with *cm1c2:gfp* in the backbone. The resultant animals were crossed to *Tg(UAS:YFP)*, and the expression was compared to in situ hybridization for *fzd9b* to identify founders that recapitulated endogenous *fzd9b* expression.

Lineage tracing experiments were visualized on a Zeiss LSM 880 with Airyscan. Representative images were produced by combining 3–4 Z-slices per scan.

Whole-mount in situ hybridization and FISH. RNA probe synthesis was carried out according to the manufacturer's recommendations using the DIG-RNA labelling kit, or the fluorescein labelling kit for FISH (Roche). Probes for *fli1a*, *rag1*, *dlla*, *dlc*, *notch1b*, *kdrl*, *cdh17*, *cmyb* and *runx1* and whole-mount in situ hybridization (WISH) protocols have been previously described¹¹. The probe for *fzd9b* was generated from the full-length cDNA. The FISH signal was developed as previously described.

FACS and qPCR. Zebrafish were dissociated using Liberase TM (Roche) and filtered through an 80-µm filter. Cells were sorted on a BD Influx cell sorter according to standard procedures. RNA and cDNA were synthesized by standard means and qPCR was performed using FastStart Universal SYBR Green Master Mix (Roche) according to the manufacturer's recommendations and shown using the 2^{-ΔΔCt} method, as previously described³. Sequences of primers are analysed in Supplementary Table 1.

Quantifying HSPCs. HSPCs were quantified by counting the number of *kdrl:mCherry*; *gata2b:GFP* double-positive cells in floor of the dorsal aorta in the region above the yolk extension in a 625-µm confocal Z-stack encompassing the entire mediolateral segment of the aorta. The number of HSPCs per millimetre was calculated from this data. Confocal images were generated by stacking 1–4 individual Z-slices. When quantifying WISH data, the number of *Cmyb*⁺ or *Runx1*⁺ cells were counted above the yolk extension.

Human embryonic stem cell culture and HSPC differentiation. All experiments described in this study were approved by a research oversight

committee (IRB/ESCRO protocol no. 100210, principal investigator: K.W.). Human embryonic stem cell H9 (WA09, NIH registration number 062) cells were obtained from WiCell. Cells were maintained in Essential 8 media, with minor modifications, as previously described⁵⁸. Plasmids encoding pools of shRNAs for FZD9 and WNT9A were obtained from ABM. The cell lines harbouring shRNAs for control, WNT9A and FZD9 were generated by lentiviral transduction, as previously described^{58,59}. Virally infected cells were selected with puromycin (4 µg ml⁻¹) and differentiated to HSPCs as previously described³⁰. Cells were dissociated and HSPCs were quantified by flow cytometry as previously described².

APEX2-mediated proximity labelling. CHO cells were stably integrated with a CMV:Wnt9a construct. Conditioned medium from CHO cells with or without this construct was collected for 2 weeks, pooled together, filtered through a 0.22-µm filter and tested for Wnt9a activity using the luciferase STF assay with Fzd9b. HEK293T cells were stably integrated with a CMV:Fzd9b-5GS-APEX2 construct. APEX2-mediated proximity labelling was carried out as described²⁷. Briefly, confluent 150-mm plates of CMV:Fzd9b-5GS-APEX2 cells were treated with biotin-phenol for a total of 30 min each, ending at the time of hydrogen peroxide treatment²⁷. Cells were treated with Wnt9a conditioned medium for 1 or 5 min, or with wild-type CHO conditioned medium for 5 min. Cells were treated with hydrogen peroxide for 1 min, quenched and lysed, and biotinylated proteins were enriched by streptavidin pull-down, as previously described.

Protein digestion. To denature the eluted proteins, an equal volume of 8 M urea in 50 mM HEPES, pH 8.5, was added to each sample. Protein disulfide bonds were reduced by dithiothreitol (Sigma) and alkylated with iodoacetamide (Sigma) as previously described⁶⁰. Proteins were precipitated using trichloroacetic acid and resuspended in 300 µl buffer (1 M urea (Fisher) and 50 mM HEPES, pH 8.5) for proteolytic digestion.

Proteins were serially digested with 30 µg LysC overnight at room temperature, then with 3 µg trypsin for 6 h at 37°C⁶¹, quenched by the addition of trifluoroacetic acid (Pierce), and peptides were desalted with C18-StageTips extraction columns (Waters) as previously described⁶¹. Peptides were dried in a speed vac, then resuspended in 50% acetonitrile/5% formic acid and quantified by the Pierce Quantitative Colorimetric Peptide Assay (Thermo); an equal amount of each sample was run on a pooled bridge channel⁶². Aliquots were dried under vacuum and stored at -80°C until they were labelled with tandem mass tag (TMT) reagents.

TMT labelling. Peptides were labelled with 10-plex TMT reagents (Thermo) as previously described⁶³. Briefly, TMT reagents were reconstituted in dry acetonitrile (Sigma) at 20 µg ml⁻¹. Dried peptides were resuspended in 30% dry acetonitrile in 200 mM HEPES, pH 8.5, and 8 µl of the appropriate TMT reagent was added to the peptides. Reagent 126 (Thermo) was used as a bridge between MS runs. Remaining reagents were used to label samples in a random order. Labelling was carried out for 1 h at room temperature and was quenched by adding 9 µl of 5% hydroxylamine (Sigma), which was allowed to react for 15 mins at room temperature. Labelled samples were acidified by adding 50 µl of 1% TFA, pooled into appropriate 10-plex TMT samples and desalted with C18 Sep-Paks.

LC-MS2/MS3 analysis. All LC-MS2/MS3 experiments were performed on an Orbitrap Fusion mass spectrometer (Thermo) with an in-line Easy-nLC 1000 (Thermo). Home-pulled, home-packed columns (100 mm inner diameter × 30 cm, 360 mm outer diameter) were used for analysis. Analytical columns were triple packed with 5 µm C4 resin, 3 µm C18 resin and 1.8 µm C18 resin (Sepax) to lengths of 0.5 cm, 0.5 cm and 30 cm, respectively. Peptides were eluted with a linear gradient from 11% to 30% acetonitrile in 0.125% formic acid over 165 min at a flow rate of 300 nl min⁻¹ and heating the column to 60°C. Nano-electrospray ionization was performed by applying 2,000 V through a stainless-steel T-junction at the inlet of the microcapillary column.

The mass spectrometer was operated in a data-dependent mode, with a survey scan performed over a *m/z* range of 500–1,200 at a resolution of 1.2 × 10⁵ in the Orbitrap. The target automatic gain control was set to 2 × 10⁵ with a maximum inject time of 100 ms and an s-lens radio frequency of 60. Top Speed mode was used to select the most abundant ions for tandem MS analysis. All data collected were centroided.

Ions above an intensity threshold of 5 × 10⁵ were isolated in the quadrupole and fragmented using collision-induced dissociation (normalized energy: 30%) for MS2 analysis. MS2 fragments were detected in the ion trap using the rapid scan rate setting with an automatic gain control of 1 × 10⁴ and a maximum injection time of 35 ms.

For MS3 analysis, synchronous precursor selection was used to maximize quantitation sensitivity of the TMT reporter ions⁶³. Up to 10 MS2 ions were simultaneously isolated and fragmented with high-energy collision-induced dissociation (normalized energy: 50%). MS3 fragment ions were analysed in the Orbitrap with a resolution of 6 × 10⁴. The automatic gain control was set to 5 × 10⁴ using a maximum injection time of 150 ms. MS2 ions 40 *m/z* below and 15 *m/z* above the MS1 precursor ion were excluded from MS3 selection.

Data processing. Raw spectral data were processed using Proteome Discoverer 2.1.0.81 (Thermo). MS2 spectra were identified using the Sequest HT node⁶⁴, searching against the Human Uniprot database (downloaded: 5 November 2017) with the zebrafish Fzd9b sequence appended. False discovery rate estimation was performed using a reverse decoy database^{65–67}. Search parameters were as follows. Mass tolerances were set to 50 ppm and 0.6 Da for MS1 and MS2 scans, respectively. Full trypsin digestion was specified with a maximum of two missed cleavages per peptide. Modifications included static 10-plex TMT tags on peptide N termini and lysine, static carbamidomethylation of cysteine and variable oxidation of methionine. Data were filtered to a 1% false discovery rate at both the peptide and the protein level.

The intensities of TMT reporter ions were extracted from the MS3 scans for quantitative analysis. Before quantitation, spectra were filtered to have an average signal-to-noise ratio of 10 across all labels and an isolation interference of less than 25%. Data were normalized in a two-step process as previously described⁶³, by normalizing each protein of the pooled bridge channel value and then normalizing to the median of each reporter ion channel and the entire data set.

Statistics and reproducibility. For APEX results, two-tailed Student's *t*-tests were used to determine significantly enriched proteins at each time point. If the variances between samples were determined to be unequal by an *F*-test, Welch's correction was used. Significantly changing proteins were prioritized using pi score⁶⁸, a metric that takes both the *P* value and the fold change into account. GO analysis of the significant proteins was performed using the database for annotation, visualization and integrated discovery (DAVID) server⁶⁹. For STF assays and qPCR or cell counting comparing more than two populations, one-way analysis of variance (ANOVA), followed by post-test analysis were conducted. For qPCR or cell counting comparing only two populations, two-tailed Student's *t*-tests were used. All data analyses and statistical findings are available in Supplementary Table 3.

Plasmids. Expression constructs were generated by standard means using PCR from cDNA libraries generated from zebrafish larvae at 24 hpf or from human embryonic stem cells; these constructs were cloned into pCS2+, downstream of a CMV promoter, and upstream of *IRES:mKate2*. Addgene provided expression vectors for *Cas9* (47929), guide RNAs (46759) and zebrafish *ctmb1* (17199).

Reagents. A list of reagents and catalogue numbers is available in Supplementary Table 2.

Reporting Summary. Further information on research design is available in the Nature Research Reporting Summary linked to this article.

Data availability

MS data have been deposited in ProteomeXchange with the primary accession code PXD010649 through MassIVE (MSV000082677). Summary data are seen in Supplementary Figs. 6e,f and 7d,e. Source data for the main and supplementary figures have been provided as Supplementary Table 3. Previously published sequencing data that were re-analysed here are available from the European Nucleotide Archive under the accession number PRJEB4197. All other data supporting the findings of this study are available from the corresponding authors on reasonable request.

References

- Fernandez, A. et al. The WNT receptor FZD7 is required for maintenance of the pluripotent state in human embryonic stem cells. *Proc. Natl. Acad. Sci. USA* **111**, 1409–1414 (2014).
- Grainger, S. et al. CRISPR guide RNA validation in vitro. *Zebrafish* **14**, 383–386 (2017).
- Kwan, K. M. et al. The Tol2kit: a multisite gateway-based construction kit for Tol2 transposon transgenesis constructs. *Dev. Dyn.* **236**, 3088–3099 (2007).
- Huggins, I. J. et al. The WNT target SP5 negatively regulates WNT transcriptional programs in human pluripotent stem cells. *Nat. Commun.* **8**, 1034 (2017).
- Moya, N., Cutts, J., Gaasterland, T., Willert, K. & Brafman, D. A. Endogenous WNT signaling regulates hPSC-derived neural progenitor cell heterogeneity and specifies their regional identity. *Stem Cell Rep.* **3**, 1015–1028 (2014).
- Haas, J. P. Measurement of infection control department performance: state of the science. *Am. J. Infect. Control* **34**, 543–549 (2006).
- Lapek, J. D. Jr, Lewinski, M. K., Wozniak, J. M., Guatelli, J. & Gonzalez, D. J. Quantitative temporal viromics of an inducible HIV-1 model yields insight to global host targets and phospho-dynamics associated with protein Vpr. *Mol. Cell. Proteomics* **16**, 1447–1461 (2017).
- Lapek, J. D. Jr et al. Defining host responses during systemic bacterial infection through construction of a murine organ proteome atlas. *Cell Syst.* **6**, 579–592.e4 (2018).
- McAlister, G. C. et al. MultiNotch MS3 enables accurate, sensitive, and multiplexed detection of differential expression across cancer cell line proteomes. *Anal. Chem.* **86**, 7150–7158 (2014).

64. Eng, J. K., McCormack, A. L. & Yates, J. R. An approach to correlate tandem mass spectral data of peptides with amino acid sequences in a protein database. *J. Am. Soc. Mass Spectrom.* **5**, 976–989 (1994).
65. Elias, J. E. & Gygi, S. P. Target-decoy search strategy for increased confidence in large-scale protein identifications by mass spectrometry. *Nat. Methods* **4**, 207–214 (2007).
66. Elias, J. E., Haas, W., Faherty, B. K. & Gygi, S. P. Comparative evaluation of mass spectrometry platforms used in large-scale proteomics investigations. *Nat. Methods* **2**, 667–675 (2005).
67. Peng, J., Elias, J. E., Thoreen, C. C., Licklider, L. J. & Gygi, S. P. Evaluation of multidimensional chromatography coupled with tandem mass spectrometry (LC/LC-MS/MS) for large-scale protein analysis: the yeast proteome. *J. Proteome Res.* **2**, 43–50 (2003).
68. Xiao, Y. et al. A novel significance score for gene selection and ranking. *Bioinformatics* **30**, 801–807 (2014).
69. Huang da, W., Sherman, B. T. & Lempicki, R. A. Systematic and integrative analysis of large gene lists using DAVID bioinformatics resources. *Nat. Protoc.* **4**, 44–57 (2009).

Reporting Summary

Nature Research wishes to improve the reproducibility of the work that we publish. This form provides structure for consistency and transparency in reporting. For further information on Nature Research policies, see [Authors & Referees](#) and the [Editorial Policy Checklist](#).

Statistics

For all statistical analyses, confirm that the following items are present in the figure legend, table legend, main text, or Methods section.

- | n/a | Confirmed |
|-------------------------------------|--|
| <input type="checkbox"/> | <input checked="" type="checkbox"/> The exact sample size (n) for each experimental group/condition, given as a discrete number and unit of measurement |
| <input type="checkbox"/> | <input checked="" type="checkbox"/> A statement on whether measurements were taken from distinct samples or whether the same sample was measured repeatedly |
| <input type="checkbox"/> | <input checked="" type="checkbox"/> The statistical test(s) used AND whether they are one- or two-sided
<i>Only common tests should be described solely by name; describe more complex techniques in the Methods section.</i> |
| <input checked="" type="checkbox"/> | <input type="checkbox"/> A description of all covariates tested |
| <input checked="" type="checkbox"/> | <input type="checkbox"/> A description of any assumptions or corrections, such as tests of normality and adjustment for multiple comparisons |
| <input type="checkbox"/> | <input checked="" type="checkbox"/> A full description of the statistical parameters including central tendency (e.g. means) or other basic estimates (e.g. regression coefficient) AND variation (e.g. standard deviation) or associated estimates of uncertainty (e.g. confidence intervals) |
| <input type="checkbox"/> | <input checked="" type="checkbox"/> For null hypothesis testing, the test statistic (e.g. F , t , r) with confidence intervals, effect sizes, degrees of freedom and P value noted
<i>Give P values as exact values whenever suitable.</i> |
| <input checked="" type="checkbox"/> | <input type="checkbox"/> For Bayesian analysis, information on the choice of priors and Markov chain Monte Carlo settings |
| <input checked="" type="checkbox"/> | <input type="checkbox"/> For hierarchical and complex designs, identification of the appropriate level for tests and full reporting of outcomes |
| <input checked="" type="checkbox"/> | <input type="checkbox"/> Estimates of effect sizes (e.g. Cohen's d , Pearson's r), indicating how they were calculated |

Our web collection on [statistics for biologists](#) contains articles on many of the points above.

Software and code

Policy information about [availability of computer code](#)

Data collection	Raw spectral data were processed using Proteome Discoverer 2.1.0.81 (Thermo).
Data analysis	<p>MS2 spectra were identified using the Sequest HT node, searching against the Human Uniprot database (downloaded: 5/11/2017) with the zebrafish Fzd9b sequence appended. False discovery rate (FDR) estimation was performed using a reverse decoy database. Search parameters were as follows. Mass tolerances were set to 50 ppm and 0.6 Da for MS1 and MS2 scans, respectively. Full trypsin digestion was specified with a maximum of two missed cleavages per peptide. Modifications included static 10-plex TMT tags on peptide n-termini and lysine, static carbamidomethylation of cysteine and variable oxidation of methionine. Data were filtered to a 1% FDR at both the peptide and protein level.</p> <p>The intensities of TMT reporter ions were extracted from the MS3 scans for quantitative analysis. Prior to quantitation, spectra were filtered to have an average signal to noise of 10 across all labels and an isolation interference less than 25%. Data were normalized in a two-step process by normalizing each protein the pooled bridge channel value and then normalizing to the median of each reporter ion channel and the entire dataset.</p> <p>Immunoblot intensities from pulldowns were quantified by densitometry using ImageJ 1.46, normalized to input controls.</p> <p>GraphPad Prism 7.04 was used for statistical analyses.</p> <p>Gene ontology of the significant proteins was performed using the database for annotation, visualization and integrated discovery (DAVID version 6.8) server.</p>

For manuscripts utilizing custom algorithms or software that are central to the research but not yet described in published literature, software must be made available to editors/reviewers. We strongly encourage code deposition in a community repository (e.g. GitHub). See the Nature Research [guidelines for submitting code & software](#) for further information.

Data

Policy information about [availability of data](#)

All manuscripts must include a [data availability statement](#). This statement should provide the following information, where applicable:

- Accession codes, unique identifiers, or web links for publicly available datasets
- A list of figures that have associated raw data
- A description of any restrictions on data availability

Mass spectrometry data have been deposited in ProteomeXchange with the primary accession code PXD010649 through MassIVE (MSV000082677). Source data for main and supplementary figures have been provided as Supplementary Table 3.

Previously published sequencing data that were re-analysed here are available from the European Nucleotide Archive under the accession number PRJEB4197

<https://www.ebi.ac.uk/ena>.

All other data supporting the findings of this study are available from the corresponding author on reasonable request.

Summary data is seen in Extended data Figs. 6e, 6f, 7d, 7e.

Field-specific reporting

Please select the one below that is the best fit for your research. If you are not sure, read the appropriate sections before making your selection.

- Life sciences Behavioural & social sciences Ecological, evolutionary & environmental sciences

For a reference copy of the document with all sections, see [nature.com/documents/nr-reporting-summary-flat.pdf](https://www.nature.com/documents/nr-reporting-summary-flat.pdf)

Life sciences study design

All studies must disclose on these points even when the disclosure is negative.

Sample size	Based on preliminary studies, we determined that examining 5-10 fish and n=3-6 for luciferase assays are sufficient for at least 95% statistical power.
Data exclusions	Samples were only excluded as outliers in the case of obvious error in instrument detection, or transfection failure. The exclusion criteria was pre-established as a zero-read on the instrument, or transfection efficiency lower than 20%, as measured by GFP+cells/total cells. Zebrafish cell counts were only excluded in case of staining failure.
Replication	To ensure reproducibility, all experiments were conducted with multiple samples, and reproduced successfully with a similar trend at least once. Replicates of luciferase assays that did not have sufficient transfection efficiency (more than 20%) did not signal. See figure legends for specific details.
Randomization	Zebrafish offspring were pooled from several clutches and separated into control or experimental groups at random for injection experiments. In the case of genetic experiments, randomization was not possible, but blinding (see below) was carried out.
Blinding	For zebrafish genetic experiments, heterozygous animals were crossed, and clutchmates were genotyped after experimental analysis (blinded). For MO injected fish, blinding was not performed. In luciferase reporter experiments, data was collected and analyzed blindly and labeled post analysis.

Reporting for specific materials, systems and methods

We require information from authors about some types of materials, experimental systems and methods used in many studies. Here, indicate whether each material, system or method listed is relevant to your study. If you are not sure if a list item applies to your research, read the appropriate section before selecting a response.

Materials & experimental systems

n/a	Involvement in the study
<input type="checkbox"/>	<input checked="" type="checkbox"/> Antibodies
<input type="checkbox"/>	<input checked="" type="checkbox"/> Eukaryotic cell lines
<input checked="" type="checkbox"/>	<input type="checkbox"/> Palaeontology
<input type="checkbox"/>	<input checked="" type="checkbox"/> Animals and other organisms
<input checked="" type="checkbox"/>	<input type="checkbox"/> Human research participants
<input checked="" type="checkbox"/>	<input type="checkbox"/> Clinical data

Methods

n/a	Involvement in the study
<input checked="" type="checkbox"/>	<input type="checkbox"/> ChIP-seq
<input type="checkbox"/>	<input checked="" type="checkbox"/> Flow cytometry
<input checked="" type="checkbox"/>	<input type="checkbox"/> MRI-based neuroimaging

Antibodies

Antibodies used

Fzd9b (1:1000, in house, rabbit polyclonal), Wnt9a (1:1000, in house, rabbit polyclonal), V5 (1:5000, genetex, mouse monoclonal)

clone GT1071, cat#GTX628529 lot 41288), phospho-Y (1:1000, BioLegend, mouse monoclonal Clone PY20, cat#309301 lot B232939), LRP6 (1:2000, cell signaling, rabbit monoclonal C5C7, cat#2560S lot 11), B-actin (1:20,000, mouse monoclonal C47E12, Sigma, cat#A2228-100UL lot 058M4808), EGFR (1:1000, abcam, rabbit monoclonal EP38Y, cat#ab52894), HBEGF (500ng/mL, R&D systems, cat#AF-259-SP lot PX101812A)

Validation

in house antibodies were validated against transfected HEK293T cell lysate.

manufacturer validations:

v5: V5-tagged-NROB1-transfected 293T western blot

LRP6: Western blot analysis of total cell lysates from HepG2, HeLa and Rat2 cells using LRP6 (C5C7) Rabbit mAb.

pTyr, actin: Each lot is quality tested in Western blot.

EGFR: western blot using A431 (human squamous carcinoma) lysate which naturally overexpresses the EGFR protein.

HBEGF: Measured by its ability to neutralize HB-EGF-induced proliferation in the Balb/3T3 mouse embryonic fibroblast cell line.

Eukaryotic cell lines

Policy information about [cell lines](#)

Cell line source(s)

WiCell (H9), ATCC (Chinese Hamster Ovary, HEK293T)

Authentication

None of the cell lines used were authenticated.

Mycoplasma contamination

All cell lines tested negative for mycoplasma contamination, with the exception of 293T TOP:FLASH reporter cells, which tested positive. This was controlled for by using the parental cells as the control group with matched levels of transfected DNA.

Commonly misidentified lines
(See [ICLAC](#) register)

HEK293 cells are known to have potential cross-contamination with HeLa cells. This was irrelevant to our study, as these cells were used only as a reporter of Wnt activity, where any cell line would be used.

Animals and other organisms

Policy information about [studies involving animals](#); [ARRIVE guidelines](#) recommended for reporting animal research

Laboratory animals

Zebrafish (Danio Rerio) were used; wild-type strain AB*, Tg(kdrl:Cherry-CAAX)y171, Tg(fli1a:eGFP)zf544, Tg(cdh5:Gal4)mu101, Tg(UAS:CA- β -catenin)sd47Tg Tg(gata2b:KalTA4sd32; UAS:Lifect:eGFPmu271), wnt9ad28/d28,sd49, Tg(UAS:Cre)t32240Tg Tg(bactin2:loxP-BFP-loxP-DsRed)sd27.

Adult fish were mated between 3-15 months of age. Offspring were generated with a male x female cross; the sex of zebrafish embryos is not readily detectable, but a 50:50 distribution is assumed. Offspring ages are noted in each figure.

Wild animals

This study did not involve wild animals.

Field-collected samples

The study did not involve samples collected from the field.

Ethics oversight

Zebrafish were maintained and propagated according to University of California and local Institutional Animal Care and Use Committee (IACUC) policies.

Note that full information on the approval of the study protocol must also be provided in the manuscript.

Flow Cytometry

Plots

Confirm that:

- The axis labels state the marker and fluorochrome used (e.g. CD4-FITC).
- The axis scales are clearly visible. Include numbers along axes only for bottom left plot of group (a 'group' is an analysis of identical markers).
- All plots are contour plots with outliers or pseudocolor plots.
- A numerical value for number of cells or percentage (with statistics) is provided.

Methodology

Sample preparation

cells were harvested with Accutase, pelleted, resuspended in PBS with 1% BSA and 1mM EDTA, filtered through an 80um filter and sorted using a BD Fortessa flow cytometer.

Instrument

BD Fortessa LSR II

Software

Flow Jo (X.0.7) and FACS Diva (6)

Cell population abundance

a minimum of 10,000 cells per sample were analyzed.

Gating strategy

Gates were set to unstained cells with no primary antibody present. All gates were compared to control samples within the same experiment, using the same gates. Gating strategy is found in extended data figures 3g-i.

Tick this box to confirm that a figure exemplifying the gating strategy is provided in the Supplementary Information.